J. Fluid Mech. (1996), *vol.* 325, *pp.* 303–330

A volumetrically heated jet: large-eddy structure and entrainment characteristics

By G. S. BHAT[1] AND R. NARASIMHA[1,2]

[1]Centre for Atmospheric Sciences, Indian Institute of Science, Bangalore 560 012, India

[2]Jawaharlal Nehru Centre for Advanced Scientific Research, Bangalore 560 094, India

(Received 22 September 1994 and in revised form 7 May 1996)

We report here an experimental study of a round vertical liquid jet that, after achieving a self-preserving state, is subjected to volumetric heating between two diametral stations. The heat injection is achieved by applying a voltage across the stations, the jet fluid having been rendered electrically conducting by the addition of acid. Using laser-induced fluorescence, digital image processing and laser-Doppler anemometry, the flow properties of the jet have been studied in detail. It is found that, with sufficient heating, the jet no longer grows linearly with height, and the decay of both centreline velocity and turbulence intensity is arrested, and may even be reversed just beyond the zone of heat addition; nevertheless the entrainment decreases, which is at variance with the hypotheses often made for modelling it. This behaviour is here attributed to the disruptive influence that, as the present experiments show, the volumetric heating has on the large-scale vortical structures in the jet, which are known to be largely responsible for the engulfment of ambient fluid that is the first step in the entrainment process. It is shown that a new non-dimensional heat release number correlates the observed data on changes in jet width. An integral model that would describe the effect of local heating is proposed, and implications for cloud development in the atmosphere are discussed.

1. Introduction

Because of their theoretical interest as well as the wide range of applications in natural and technological fluid dynamics, the entrainment of ambient fluid by jets, plumes, thermals and forced plumes (also called buoyant jets) has been extensively explored (e.g. Turner 1973, 1986; Townsend 1976; Hunt 1993). The entrainment hypothesis, which was first conceived by G. I. Taylor, postulates that the mean inflow velocity across the edge of a free turbulent shear flow is proportional to a characteristic velocity within the flow. (This is usually taken as the local time-averaged maximum mean velocity at the level of inflow (Morton, Taylor & Turner 1956), but if the flow is self-preserving it does not matter which velocity is chosen.) Basically such a hypothesis provides a closure assumption for the (integral) equations governing these flows. Several attempts have been made in the past to relate the proportionality constant, called the entrainment coefficient, to the flow conditions (e.g. Fox 1970; Hirst 1972; List & Imberger 1973); while there is no general agreement on the precise form of the relationship, the common premise among these studies is that buoyancy, when present, enhances entrainment. This is incorporated in the proposed relations not only in the fully developed part of the turbulent flow (e.g. Fox 1970; List & Imberger 1973) but also in the zone of flow establishment (in which the

mean flow profiles undergo a transition from their starting or initial conditions to those characteristic of fully turbulent flow, Hirst 1972, and are therefore not yet in a self-preserving state). All these studies imply that the entrainment mechanism is more efficient in buoyancy-driven than in momentum-driven flows. This seems *a priori* reasonable because the buoyancy force can accelerate the flow and is capable of continuously generating shear through the baroclinic torque.

However, there are certain flows, in particular those in which the buoyancy is created away from the source of origin of the flow, which are found to exhibit behaviour that is at variance with the above-mentioned results. For example, in an experiment to measure the entrainment rate in axisymmetric turbulent jets, Ricou & Spalding (1961) observed that, when the injected gas burns in the jet, the entrainment rate was up to 30% lower than when it does not. Hermanson & Dimotakis (1989) conducted experiments in a planar gas-phase reacting mixing layer formed between two free streams, and found that the growth rate of the mixing layer decreases slightly with increased heat release (by about 15% for a mean density reduction in the layer of 40% below its nominal cold value). Although normalized temperature profiles across the flow showed little change in shape, overall entrainment into the layer was substantially reduced as a result of heat release (up to a maximum of 50%).

A cumulus cloud is an example of a naturally occurring flow in which buoyancy is generated away from the source, in this case due to latent heat release during the condensation of water vapour. Models that assume entrainment of ambient air into clouds from the lateral edges and employ an entrainment relationship of the kind referred to above have failed to make realistic predictions of either liquid-water concentrations or height of penetration for the cloud (Squires & Turner 1962; Warner 1970). Some hint that the entrainment of ambient air from the sides may be very small in tall cumulus clouds was provided from an analysis of aircraft-measured temperature and liquid-water concentrations in tall Colorado cumuli by Paluch (1979). This study showed that the observed cloud thermodynamic properties can be accounted for only if air from the cloud base ascends to the cloud top without laterally mixing with the surrounding air. Another example is cumulonimbus clouds over the tropical oceans. The observed height reached by these clouds suggests that the air in these clouds must be ascending with very little lateral mixing (Riehl 1979, pp. 158–159). It may be recalled here that air accelerates above the cloud base owing to buoyancy increase in these clouds (e.g. Ludlam 1980), with a consequent increase in the shear; however, the lateral entrainment decreases drastically, and there has been no clear explanation for this behaviour. Indeed, questions concerning entrainment, mixing and detrainment in cumulus clouds form areas of active current research (see e.g. Emanuel 1994, p. 204).

It may be noted here that Taylor's entrainment hypothesis has been very successful in predicting many practical flows, including those in stratified media and several geophysical applications (see Turner 1986 for a summary); but in flows in which buoyancy is created away from the source, upsetting a previously prevalent equilibrium state, the hypothesis does not appear to be valid. Emanuel (1994, p. 540) points out how early cloud parameterization schemes were "based on the similarity entraining plume model, which was later thoroughly discredited by observations." (For an interesting review of earlier ideas, see Simpson 1983.) However, the literature does not provide an understanding of this anomalous behaviour, and there is need for a detailed study of flows with locally enhanced or created buoyancy.

The experiments reported here were undertaken to improve our understanding of flows with such (local) buoyancy increase. The present investigation forms part of a programme being pursued at the Centre for Atmospheric Sciences in Bangalore over

the last six years with the objective of shedding light on entrainment processes in clouds. Earlier experimental work on flows with heat release has invariably *depended* on mixing to produce the heating (through chemical reactions), whereas the issue is the *effect* on mixing of a heat release that takes place independently of it. A novel method of injecting heat in a liquid flow, independent of the mixing, was developed for this purpose (Bhat, Narasimha & Arakeri 1989). A detailed description of the experimental techniques adopted, along with an account of a series of exploratory studies, will be found in Elavarasan *et al.* (1995). In the present paper, we present an analysis of the results on the structure of the flow from visualizations using the laser-induced fluorescence technique, on scalar concentration widths using digital image processing, and on the axial component of velocity obtained from a laser-Doppler velocimeter.

A new parameter correlating the experimental data is proposed and an integral approach that takes into account the present experimental findings is formulated.

In the flow that is the subject of the present investigation, buoyancy comes into play only in the far field of the jet where it has reached a state of self-preservation or equilibrium; this equilibrium is disturbed because of the heating. The study demonstrates that the jet behaviour with local volumetric heating is markedly different from that of classical jets, plumes and buoyant jets. In particular in the upper part of the heat injection zone and in the regions immediately above it, the jet spread rate decreases and entrainment either drops substantially or even ceases altogether. This behaviour is here related to the considerable modification or even destruction of the coherent vortical structures in the jet that laboratory investigations in turbulent shear flows have recently shown to be largely responsible for entrainment (Roshko 1976, 1993; Broadwell & Breidenthal 1982; Hussain 1986).

The paper is organized as follows. Section 2 contains a brief description of the flow and the relevant non-dimensional parameter that we propose governs it. Section 3 gives a brief description of the experimental arrangement including the method of heating adopted. Section 4 presents experimental results, §§5 and 6 an analysis of the experimental data using an integral approach, and §7 some thoughts on the mechanism possibly responsible for the disruption of the jet eddy structures. Section 8 discusses a possible scenario for cloud development in the light of the present experiments and §9 concludes the paper.

2. Locally heated jet

2.1. *Flow arrangement*

A schematic of the flow configuration is given in figure 1. The flow is basically a standard vertical axisymmetric jet till it reaches the height $z = z_b$. Heat is added (volumetrically) in the region $z_b < z < z_t$. The buoyancy flux (weight deficit per unit time), which is proportional to the increase in temperature ΔT of the jet fluid, increases from zero at $z = z_b$ to a maximum value at $z = z_t$. For $z > z_t$, the net buoyancy flux remains constant.

For convenience, the following nomenclature has been used to refer to different regions of the jet. The neutral jet region, i.e. $z < z_b$, will be called the pre-heating zone, the region $z_b < z < z_t$ in which heat is added to the flow is the heat-injection zone and the region above this is the post-heating zone.

2.2. *Non-dimensional heating parameter*

We propose here a non-dimensional number that governs the behaviour of such a locally heated jet.

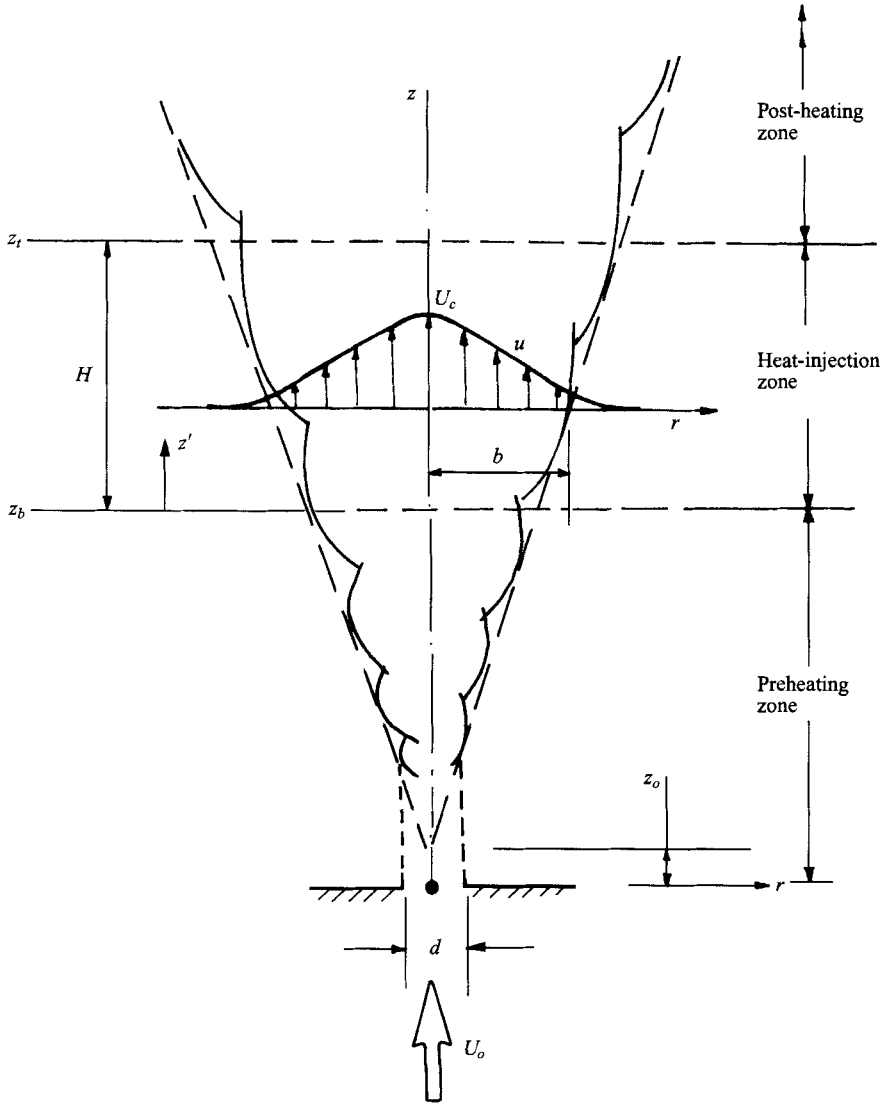

FIGURE 1. A schematic of the flow configuration.

The variables in the problem (neglecting molecular viscous effects) can be listed as follows (figure 1):

geometric : d, z, H, z';

flow : U_b, b_b, Q;

physical : ρ, c_p, α, g.

Here d is the diameter of the nozzle from which the jet issues, $z' = z - z_b$, $H \equiv z_t - z_b$ is the height of the heat-injection zone, U_b and b_b are respectively velocity and length scales at $z = z_b$, Q is the net heat addition rate (Watts), ρ is the density of the (unheated) fluid, c_p is the specific heat at constant pressure, α is the coefficient of thermal expansion and g is the acceleration due to gravity. Further, it is assumed (with the application to clouds in mind) that $H/b_b \sim O(1)$.

Because of the numerous variables in the problem, several non-dimensional groups

can be conceived. A complete description of the possibilities is not attempted here. Heuristically we postulate that the ratio of buoyancy force to the inertial force is an important parameter in the problem (as is also suggested from the momentum equation under the Boussinesq approximation). Now the buoyancy force is characterized by

$$-g\frac{\Delta\rho}{\rho} = g\alpha\Delta T, \tag{1}$$

where $\Delta\rho/\rho$ is the fractional change in density resulting from an increase in temperature ΔT of the jet fluid due to heating. A measure of the increase in temperature is given by

$$\Delta T \sim \frac{Q}{\rho c_p b_b^2 U_b}. \tag{2}$$

The inertial force is of order $\rho U_b^2/b_b$. Combining (1) and (2), a measure of the ratio of buoyancy to inertial force is

$$G' \sim \frac{g\alpha Q}{\rho c_p b_b U_b^3}. \tag{3}$$

Now in the experiments z_b/d is generally large (> 100), so the flow may be assumed to be self-preserving (and this is supported by the measurements) when it enters the heat-injection zone. The variables b_b and U_b in equation (3) can then be expressed in terms of jet inlet conditions and axial distance z using relations valid for a self-preserving axisymmetric jet, namely $b \sim z$, $U \sim z^{-1}$ (e.g. Townsend 1976). Doing this and rearranging (3), we get the more convenient non-dimensional group

$$G = \frac{\alpha g}{\rho c_p}\,\frac{z_b^2}{d^3}\,\frac{Q}{U_o^3} \tag{4}$$

where U_o is the velocity at the nozzle exit ($z = 0$). Although the numerical magnitudes of (3) and (4) differ substantially, the two are strictly proportional to each other if (as in the present experiments) the jet is self-preserving before it experiences heating. The parameter as written in (4) is preferred here because it contains quantities like d, z_b and U_o which are accurately known for each experiment. In either form, the proposed non-dimensional group is analogous to a bulk Richardson number, and is a non-dimensional heat addition rate. In the present experiments, G was varied by varying Q and U_o, while other parameters remained fixed.

3. Experimental arrangement

3.1. *Basic set-up*

Details of the basic experimental arrangement and method of heating are given in Bhat *et al.* (1989) and Elavarasan *et al.* (1995), so here the arrangement is only briefly described (figure 2). The reservoir into which the jet issues is a glass tank of dimensions 600 mm×600 mm×1200 mm (height). The tank is filled with filtered and deionized water and the jet enters from the bottom through an 8 mm dia. nozzle after undergoing an area contraction of 25. However, in most of the experiments reported here, a suitably designed cap was fitted inside the nozzle so that the actual diameter of the jet at the nozzle exit was 1.5 mm. The lowest heating electrode was located at $z_b = 200$ mm, so this gives $z_b/d = 133$.

Volumetric heating of the jet fluid was carried out by rendering it electrically

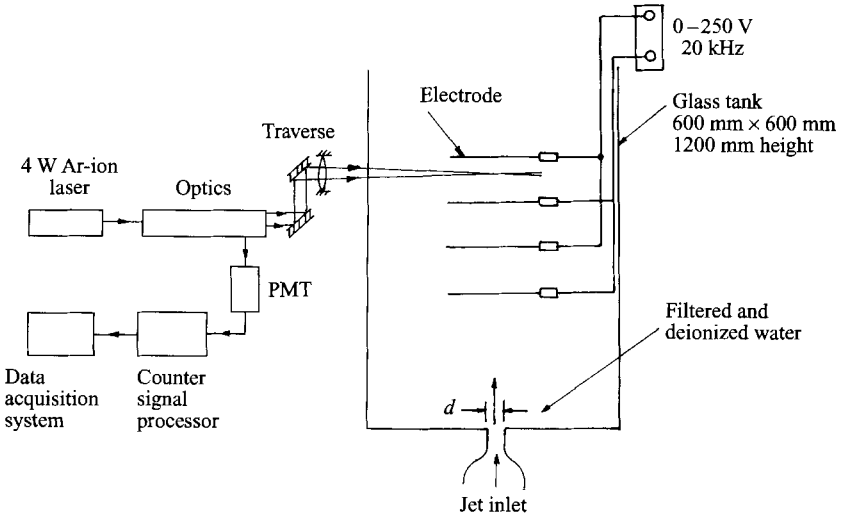

FIGURE 2. A schematic of the experimental arrangement.

conductive and applying a high-frequency (20 kHz) alternating voltage between electrodes placed horizontally across the flow at desired heights. The electrical conductivity was obtained by adding a small quantity of HCl (~2 ml per litre of water) to the jet fluid, the resulting increase in density being neutralized by adding an appropriate amount of acetone. Electrodes were made of fine platinum wire (90 μm dia.) netted on a rectangular supporting frame whose inside open area was 200 mm×200 mm. The wire Reynolds numbers are so low (< 10) that the presence of the grid does not influence flow development in the jet. It was found necessary to place more than two electrodes in the flow for injecting adequate quantities of heat into the jet: in the experiments reported here five electrodes were used with alternate ones connected in parallel. The amount of heating was easily controlled by varying the voltage across the electrodes, but the maximum was limited to about 1200 W, as at higher heating rates electrolysis occurred within a few minutes of commencing the heat injection.

One problem that appeared to adversely influence the measurements was that of jet oscillation. After reaching the top of the tank, the jet fluid curls back and induces a large-scale circulation in the tank. The direction of this circulation may change slowly with time as the jet sways from one side of the vertical to the other and so sets up an oscillation. The large eddies in the jet tend to maintain their circulation even after reaching the top; since their arrival there occurs more or less randomly in lateral position and time, the induced circulation is not steady. This problem was overcome to a large extent by heating a small layer of water at the top (Vishwanath, Narasimha & Prabhu 1978), which was about 400 jet nozzle diameters above the nearest measuring point. Heating creates a stable stratification that absorbs kinetic energy, thus reducing the slow oscillation of the jet. Too strong a stratification is of course not desirable as it could alter flow conditions; the minimum amount of stabilizing heat necessary was determined by means of flow visualization. With this arrangement, experiments could be carried out for about 15 minutes without the flow being noticeably influenced by the recirculation.

During the early stages of the flow visualization experiments, it was noticed that the

height at which the jet becomes turbulent varied from experiment to experiment. This is not surprising because, being a free shear flow, the jet is very sensitive to external disturbances, especially at low Reynolds numbers (1000 to 3000 in these experiments). This undesirable feature was overcome to some extent by a mild vibration of the set-up, induced by a motor-driven stirrer inside a constant-temperature bath vessel kept on the same platform on which the tank was placed: the weak disturbance so produced was enough to ensure that, for a given inlet velocity U_o, the jet became turbulent at about the same height on any day. This simple procedure improved jet flow reproducibility substantially. The stirrer motor frequency is close to 23 Hz, much higher than the typical eddy turnover frequency of 1–2 Hz in the heat-injection zone. The flow in this region is therefore unlikely to be influenced by the imposed vibration. Jet growth near the exit could be affected (Gutmark & Ho 1983), but the achievement of a self-preserving state shows that this is not an issue here; in any case our main objective is to compare heated and unheated cases having more or less identical conditions at the beginning of the heat injection zone.

3.2. *Flow visualization and recording*

We employ the laser-induced fluorescence (LIF) technique, with Rhodamine 6G as the dye to visualize two-dimensional sections of the jet flow. A 4 W Ar-ion laser, and a combination of spherical lenses and a cylindrical lens, were used to produce a laser light sheet with a thickness of about 300 μm in the region where the jet sections were visualized. Still photographs were taken either with a Nikon (Model EM, SLR, automatic) or Yashica (Model FX3, SLR, manual) camera. For video recording, a National make (model NV-M5EN) VHS video camera was used with a recording speed of 30 frames/s.

For calculating the dye concentration width, the video tape was played back on a VCR and the images of the jet sections were fed to an image digitizer. The digitizer unit consisted of a video decoder-encoder board to convert PAL colour signal into RGB signal and vice versa (supplied by Data Translation, USA, model DT2869) and a colour frame grabber board (model DT2871), both mounted inside an IBM PC/AT 386 system. The digitized colour image is stored in three on-board frame buffers with 512×512 pixel resolution and 8-bit accuracy. A discussion of possible errors in the estimation of jet width from the present measurements is provided in the Appendix.

3.3. *Velocity measurements*

The jet centreline velocity has been measured using a two-colour four-beam laser-Doppler velocimeter (LDA) (TSI model No. 9100-7). To improve the measurement accuracy, one of the two beams that measure the axial component of velocity is frequency-shifted using a Bragg cell. Counter-type signal processors have been used and the output from the counters is fed to a data acquisition system which stores the velocity information on a hard disk for later analysis.

4. Results

Velocity measurements acquired in the present apparatus have been presented by Elavarasan *et al.* (1995); we discuss here some salient features of the data that are important for understanding issues connected with entrainment.

First data on the unheated jet show that the flow follows the self-preserving solution very closely; present measurements of centreline velocity, jet width and turbulence intensity, summarized in table 1, are in excellent agreement with the recent work

Quantity	Hussein *et al.*	Wygnanski & Fiedler	Present apparatus
Re	9.55×10^4	$\sim 10^5$	$1.3 - 3.2 \times 10^3$
db/dz	0.094	0.086	0.09
u_c'/U_c	27%	28%	$25 \pm 2\%$
B_u	5.8	5.7, $z/d < 50$	5.7, $z/d < 100$
		5.0, $z/d > 50$	5.3, $150 < z/d < 270$
z_0/d	4	3, $z/d < 50$	~ -4, $z/d < 100$
		7, $z/d > 50$	15, $150 < z/d < 270$

TABLE 1. Selected flow parameters in unheated axisymmetric jets: b = half-width. B_u is defined by $U_c/U_0 = B_u d/(z - z_0)$.

of Hussein, Capp & George (1994). Hussein *et al.* emphasize the importance of a large enclosure in ensuring self-preservation over large distances, the dimensions in their set-up being $192d \times 192d \times 984d$, with the jet exit located at $408d$ from the end wall. This may be compared with our reservoir whose volume is $400d \times 400d \times 800d$, with the jet issuing from the end wall. Not surprisingly mean velocity profiles all collapse to a curve of nearly the same shape when scaled on local centreline velocity and jet width (Elavarasan *et al.* 1995). Similarly the centreline turbulence intensity $\hat{u}_c'$ (r.m.s. logitudinal velocity fluctuation) achieves a value of 0.25 ± 0.02 in the present experiments, close to the value 0.27 obtained in the LDA data of Hussein *et al.*

We now consider the effect of heating.

4.1. *Flow visualization*

Photographs of vertical and horizontal sections of the jet, taken on a Kodak 1600ASA colour film with an exposure time between two to four milliseconds, are shown in figures 3 and 4 respectively. In these experiments, the jet inlet velocity is constant ($1\ \mathrm{m\,s^{-1}}$) and the heating rate is varied. Figure 3(*a*) shows an instantaneous vertical section of the unheated jet (the thin horizontal lines in the pictures are due to the supporting frames of the electrode wire grids; it is incidentally seen that the grids have no noticeable effect on the structure of the flow). The brighter regions contain the (original) jet fluid whereas the darker regions indicate ambient fluid; even in the vicinity of the jet axis there are some dark regions implying the presence (through engulfment) of essentially unmixed ambient fluid there. It is seen that the jet is dominated by large eddies, and the instantaneous structure is far from being smooth. Figure 3(*a*) is consistent with previous visualizations (Dimotakis, Miake-Lye & Papantoniou 1983; Papantoniou & List 1989). As is well known, coherent structures in a jet are not as unambiguously evident from flow visualization as they are in say mixing layers. Nevertheless, detailed correlation measurements using hot wires (Tso & Hussain 1989) do show the presence of such structures, indeed of several types, the dominant being helical (double helices and rings being not so frequently encountered). Dahm & Dimotakis (1990) also report spiral-type structures. The large eddies seen in figure 3(*a*) are basically responsible for turbulent entrainment, i.e. they bring the ambient fluid into the jet (Dahm & Dimotakis 1990).

The jet section at $G = 1.8$ (corresponding to a heating rate of 330 W at $U_o = 1\ \mathrm{m\,s^{-1}}$) is shown in figure 3(*b*). The structure of the pre-heating zone is similar in nature to that seen in figure 3(*a*). In the heat-injection zone, however, the eddies are now not as sharply defined. The horizontal extent of the large eddies has diminished, and the lateral growth is clearly inhibited. Furthermore, the region near the jet axis is more

nearly uniform, indicating less engulfment. To sum up, the jet eddy structure has been disrupted in the heat-injection zone, with the immediate consequence that the entrainment of the ambient fluid into the jet is weaker.

Figure 3(*c*) shows a jet section at $G = 3.9$ ($Q = 715$ W and $U_o = 1\ \mathrm{m\,s^{-1}}$). With the increased heating rate, the eddy structure has been disrupted further and a tendency for the jet to narrow towards the top of the heat-injection zone is seen. Figure 3(*d–g*) shows four realizations of the vertical section at $G = 3.3$, covering both sides of the heat-injection zone, in order to provide an indication of the variability in the flow. It can be seen that some suggestion of a helical structure is occasionally present in the pictures. However, an important feature of the flow common to all the realizations is that, immediately above the heat-injection zone, instabilities begin to reappear in the outer region of the jet and gradually extend to the jet axis. This behaviour is somewhat similar to that observed in the zone of flow establishment where the instability of the shear layer leads to the generation and growth of large vortical structures (Hirst 1972; Liepmann & Gharib 1992). It has been observed that the extent of the zone of flow establishment in the post-heating zone is about two to three times the jet width at the top of the heat-injection zone.

Changes in the jet structure may also be clearly seen in diametral sections of the jet, presented at three heights (all for the flow with $G = 3.3$) in figure 4. The sections shown are taken respectively at the midpoints between the lowest two and the top-most two electrode grids, and at 30 mm above the heat-injection zone. At all the three heights, the unheated sections are similar and show a sharp jet boundary. Heated cases show a continuous change. The outer edge of the heated jet has changed at the lowest section (figure 4*a*). Near the top of the heat-injection zone (figure 4*b*), the change in the structure of the heated jet is very striking compared to the unheated case. Above the heat-injection zone, incipient re-emergence of an eddy structure and a more sharply defined jet boundary are seen (figure 4*c*). The flow in the post-heating zone is tending towards that in a buoyant jet. The disruption of the eddies is thus a phenomenon that is most marked within the region of volumetric heating.

In order to examine the change in the rate of entrainment more clearly, slightly buoyant and viscous dye (a mixture of water, acetone, glycerine and Rhodamine B) was released at a few points in the ambient water at a height of 70*d* above the nozzle exit. The outcome of this experiment is shown in figure 5. Figure 5(*a*) shows the bending and rolling up of the streaklines associated with the turbulent engulfment/entrainment in the unheated jet. Figure 5(*b*) shows that when the jet is heated, the rolling-up action is absent especially in the upper part of the heat-injection zone where the disruption of the eddies is the strongest.

4.2. *Scalar jet width*

Digital image processing of the video recordings of the jet sections can provide measures of the width of the scalar (i.e. acid/dye) concentration distribution across the jet. The video tape containing the recorded jet vertical sections is played back on a VCR, and the images are fed to the image processing unit. In general, the intensity buffer has been accessed, and the average brightness distributions along the horizontal sections have been obtained. The results presented here are averages over not less than 1600 frames, the corresponding experimental duration being between 3 and 4 minutes.

To determine the jet width, the average intensity at each section is first normalized by its local maximum and the pixel distance from the jet axis where this normalized intensity crosses the 1/e value is found by interpolation on either side; the average

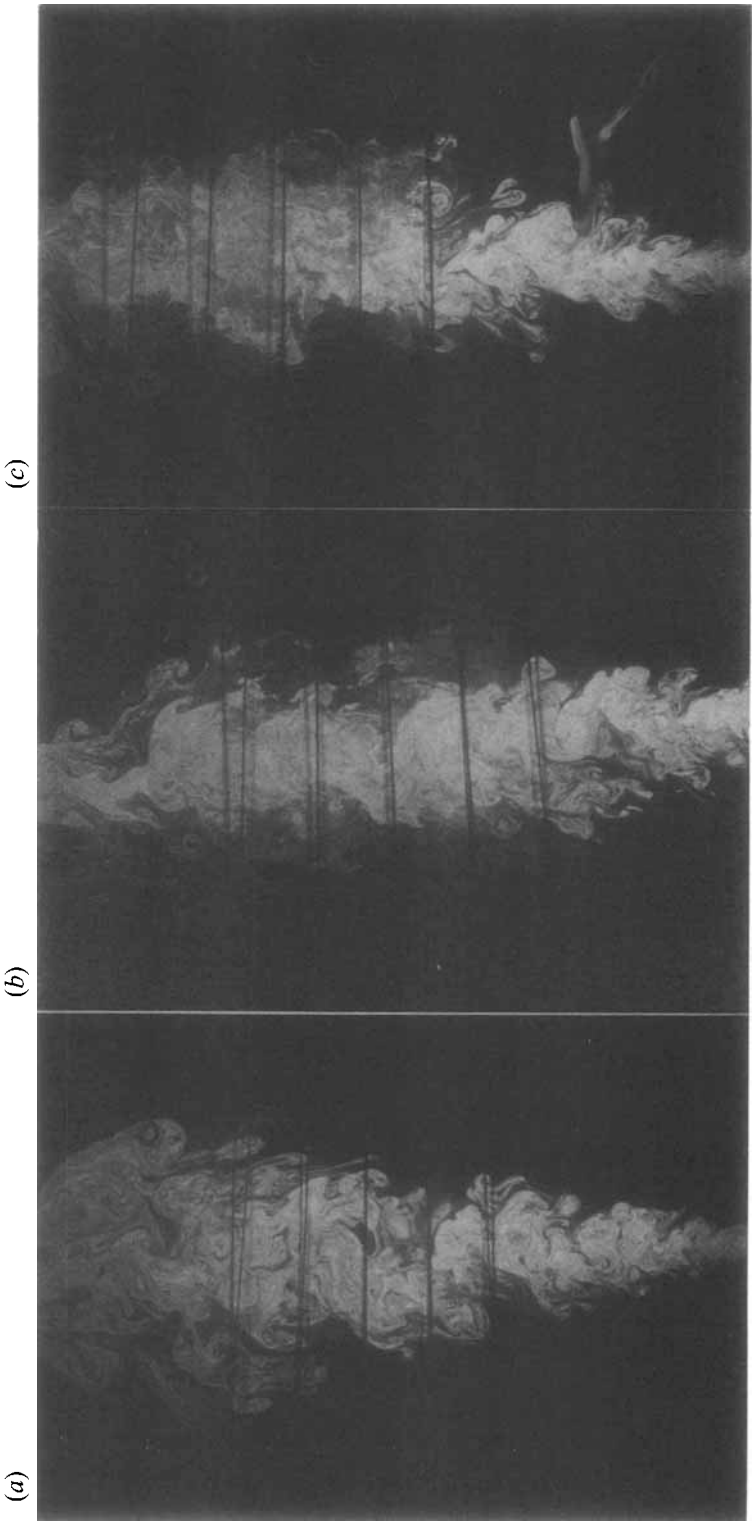

FIGURE 3 (*a–c*). For caption see facing page.

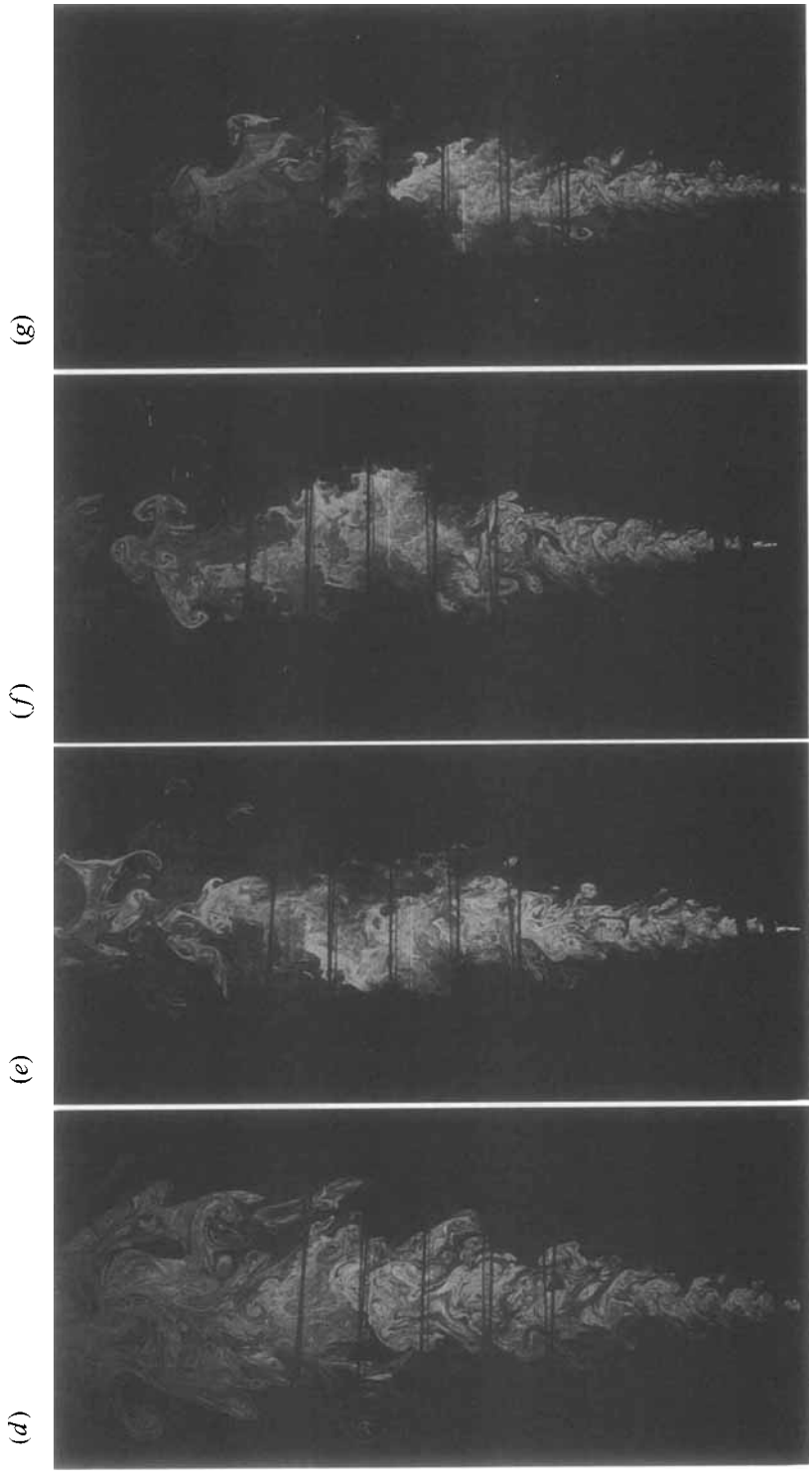

FIGURE 3 (*a–c*). Vertical sections through the jet at jet inlet velocity of 1 $m\,s^{-1}$, with increasing heating. (*a*) Unheated jet, $G = 0$. Heated jet: (*b*) $G = 1.8$, (*c*). $G = 3.9$. (*d–g*). Variability in vertical sections through jet. (*d*) Unheated jet, $G = 0$. (*e–g*) Sections at different instants, $G = 3.3$.

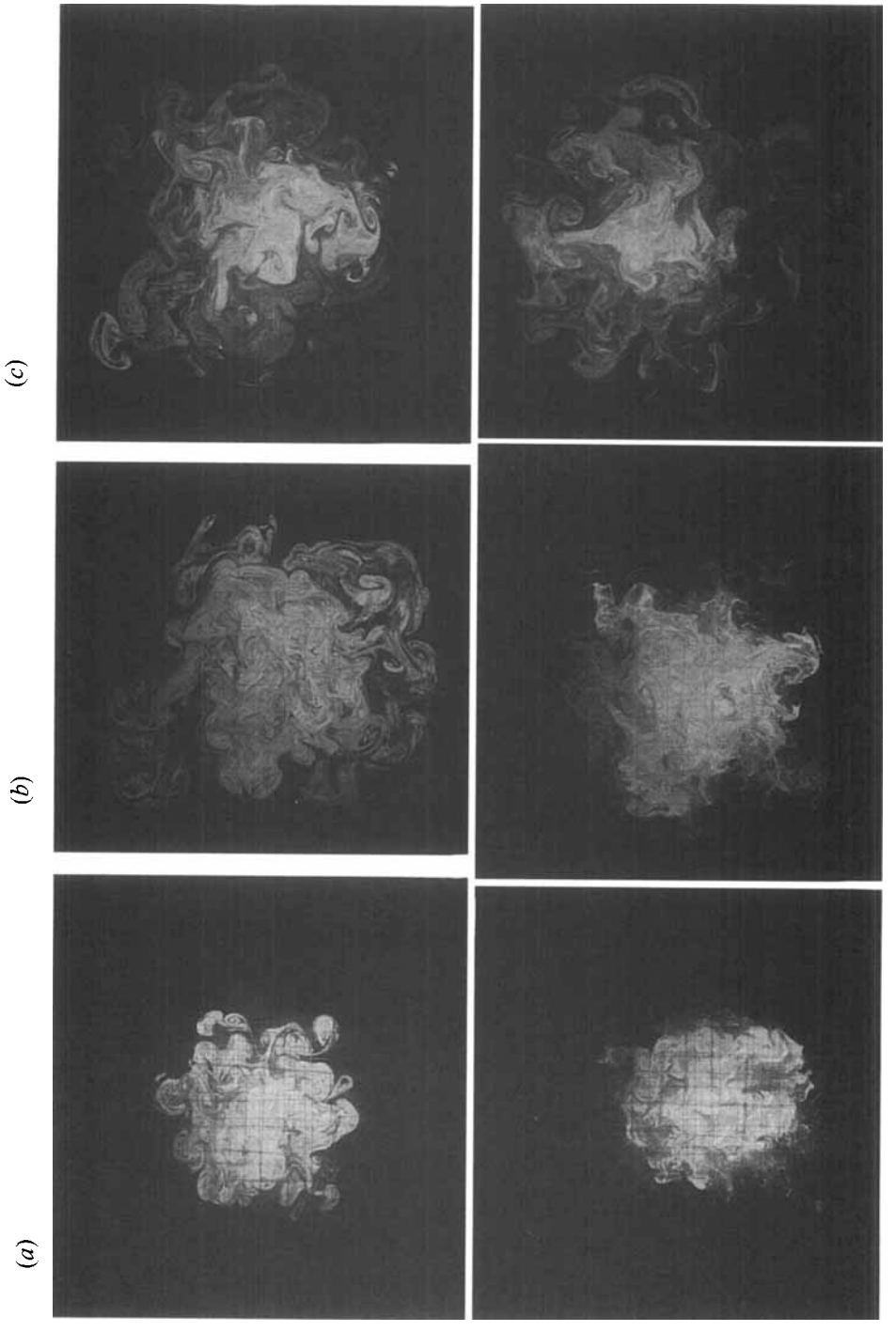

FIGURE 4. Horizontal sections of the unheated (top) and heated (bottom) jets at $G = 3.3$. (*a*) $z/d = 143$, (*b*) $z/d = 203$, (*c*) $z/d = 233$.

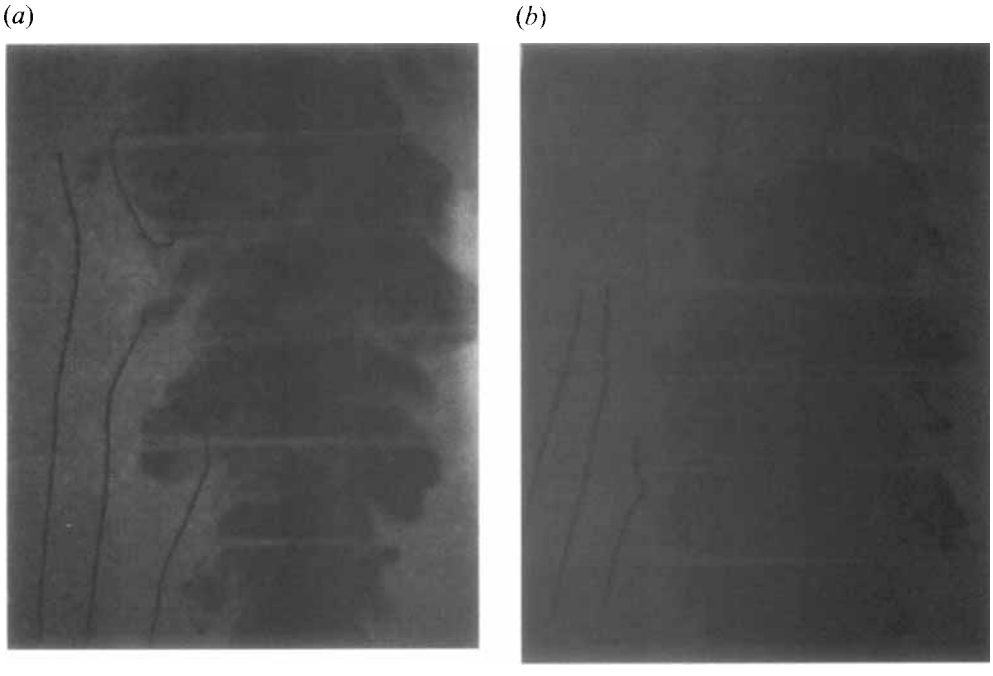

FIGURE 5. Initially vertical streaklines in the neighbourhood of the jet. (*a*) Unheated jet. (*b*) Heated jet $G = 3.3$.

of the two is taken as the local jet width in pixel units. Then the pixel distance is converted into physical distance by multiplying it by the horizontal resolution. The resolution (in either the horizontal or the vertical direction) is obtained by measuring the number of pixels in the respective direction that corresponds to some known distance in the experimental set-up (for example the spacing between electrodes).

Now the intensity measured by the image processing system is proportional to the fluorescence intensity, which, for a given optical arrangement, is in turn proportional to the dye concentration if the exciting light intensity I_e and the quantum efficiency ϕ can be assumed to be constants (see the Appendix). Even though such an assumption is not strictly valid in the present experiment, by normalizing the measured intensity by its centreline value the effect of their variation on the estimation of dye-concentration width is found to be less than 2.5% for the present experimental conditions, as shown in detail in the Appendix. Therefore, the jet width measured by the image processing system can be taken to be a proxy for the dye concentration width.

Figure 6 shows the variation of jet width with axial distance for five values of G. This figure shows that in the pre-heating zone, there is no noticeable effect of the volumetric heating, and the spread rates are the same for all values of G. Immediately after entering the heat-injection zone, there is an increase in the spread rate which appears to increase with G. However, the jet width in the upper heat-injection and post-heating zones is smaller for larger G, and the spread rate is indeed nearly zero if not slightly negative at the largest values of G.

It may be noted that in figure 6 the jet widths in the preheating zone do not strictly lie along a smooth curve, although the departure is always small. Scalar concentration widths measured by Papanicolaou & List (1988) also exhibit some spatial variation even at values of z/d larger than 100 at a Reynolds number of about 11 000. While

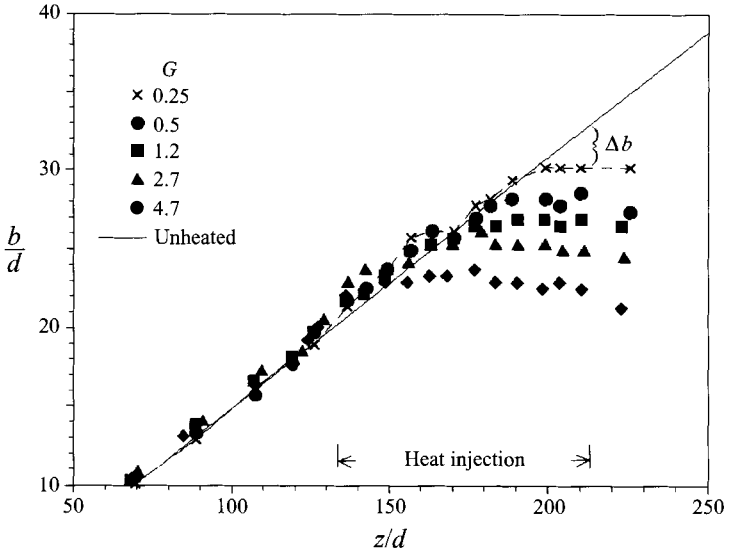

FIGURE 6. Streamwise variation of scalar jet width b at different values of the heating parameter G.

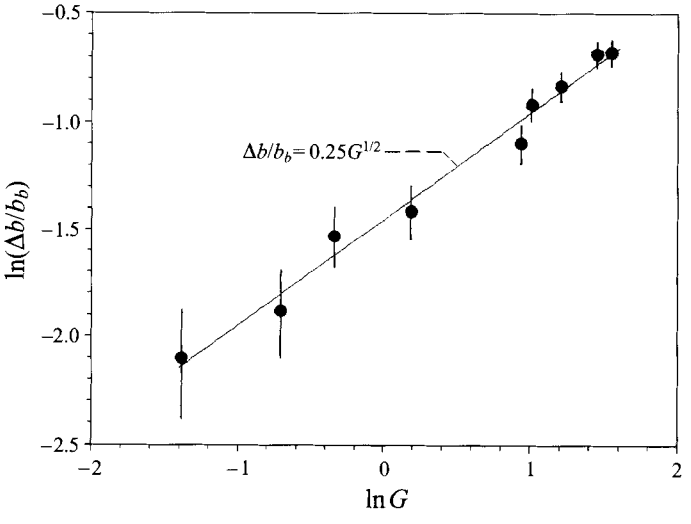

FIGURE 7. Dependence on G of the difference Δb between unheated and heated jet width at z_t (normalized by b_b, the jet width at z_b).

experimental errors are one possible source of these deviations, another is that the jet flow is not completely random and may contain spatially coherent structures embedded at particular positions in the turbulent flow. This however does not affect the major features of the flow development in the jet.

The difference in jet width with and without heating at different axial positions provides one gross measure of the effect of the heating on the flow. From figure 6 it can be seen that this difference depends on $z'(= z - z_b)$ and G. Let us consider the top of the heat-injection zone, i.e. $z' = H$, and denote the difference in width there by Δb. The variation of Δb (normalized by b_b, the jet width at $z = z_b$) with G is shown on a log-log plot in figure 7. The uncertainty in estimating b, associated with manually

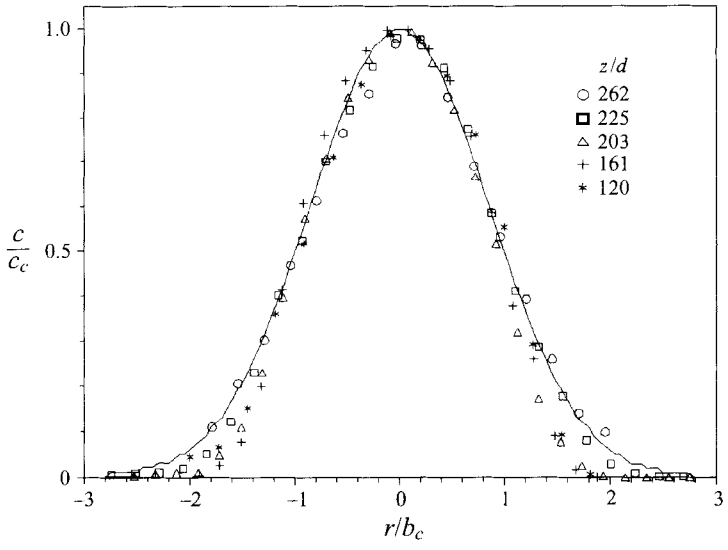

FIGURE 8. Dye concentration profiles at different stations in the heated jet at $G = 4.7$. The line is the Gaussian distribution.

fitting the lines and measuring Δb, is about $\pm$ 1 mm. It is seen that over the range of G considered here, points lie close to a straight line with a mean slope of 0.5. In this region, Δb is thus approximately given by

$$\Delta b = 0.25\, b_b\, G^{0.5}. \tag{5}$$

This relationship clearly cannot be valid for very large values of G as the jet cannot narrow indefinitely.

Figure 8 shows the horizontal distribution of dye concentration at $G = 4.7$ and at five axial locations. A Gaussian distribution describes the shape fairly well in the central region of the jet, but towards the edges the experimental points fall off more rapidly.

4.3. *Velocity distribution*

Figure 9(*a*) shows the variation of the axial component of velocity along the jet axis. It is seen that at high heating rates and low jet inlet velocity, the jet accelerates slightly in the upper heat-injection and post-heating zones. Figure 9(*b*) shows the turbulence intensity along the jet axis. It is seen that as G increases, the normalized intensity u'/U_c experiences a drastic reduction (by about 35%) in the early part of the heat-injection zone, and thereafter seems to reach an asymptotic value of about 16%. On the other hand the unnormalized intensity u'_c at the highest G is nearly twice that in the unheated jet at $z/d \simeq 400$ and 450! Even the normalized intensity shows indications of increasing again in the post-heating zone for large values of G, and could be tending towards the equilibrium value in a plume, but at the two lower values of G the normalized intensity is still falling, indicating a very slow relaxation. (The slow relaxation is consistent with experience in other free shear flows, e.g. the wakes studied by Narasimha & Prabhu 1972.)

The distribution of the axial component of velocity across the jet has been measured at a few axial stations, and shows no noticeable change in profile shape with heating in the central part of the jet (figure 9*c*; a more detailed report will be found in Elavarasan *et al.* 1995). A Gaussian distribution describes the shape fairly well in

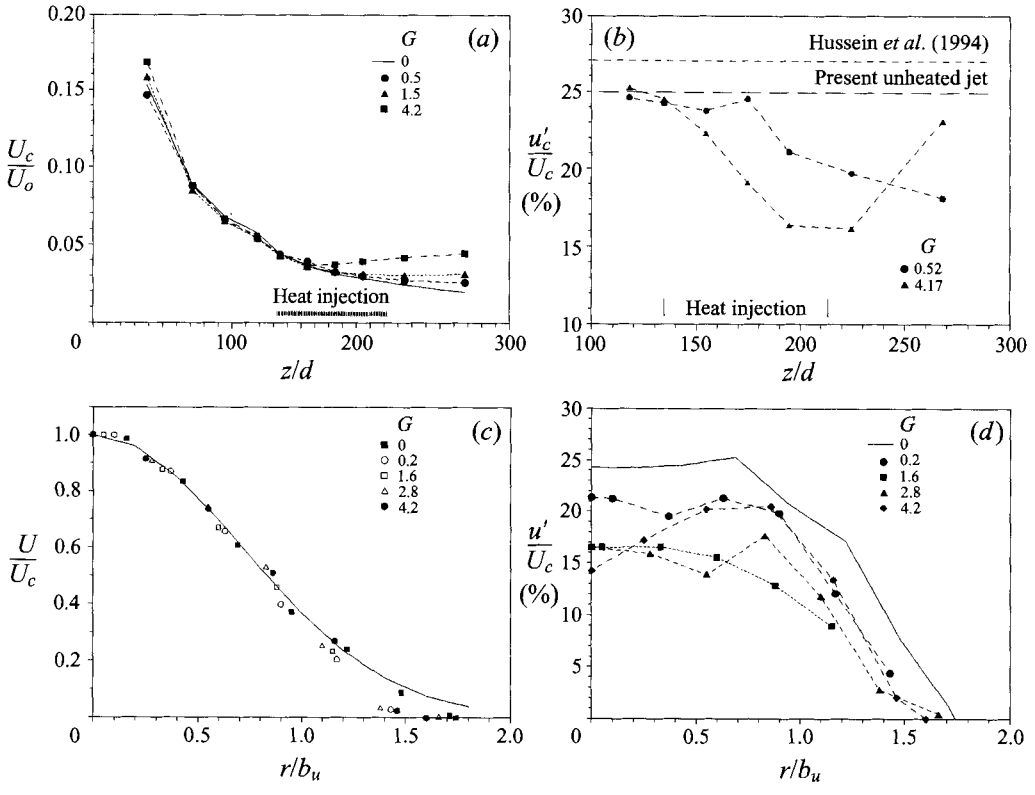

FIGURE 9. (*a*) Variation of the mean velocity at the centreline along the jet axis as a function of G. (*b*) Normalized turbulent intensity along the jet axis as a function of G. (*c*) Profile of the mean axial component of velocity as a function of G at $z/d = 225$ (a little above the heated-injection zone). The line is the Gaussian distribution. (*d*) Profile of turbulent intensity, same conditions as (*c*).

the central region of the jet, but towards the edges the experimental points generally fall off rapidly, more so in the heated jet. The turbulence intensity (figure 9*d*) shows larger variability with heating and the normalized profile is narrower in the heated jet.

4.4. *Discussion of experimental results*

The results presented in the previous subsections demonstrate that volumetric heating modifies the flow considerably. A noticeable feature is the disruption of the jet vortical structure in the heat-injection zone, and a zone of flow re-establishment in the lower post-heating zone. Visual observations and quantitative measurements of jet width using digital image processing show a drastic reduction in the jet spread rate upon heating. The departure of the heated jet width from that of the neutral jet at a given axial distance depends on the parameter G; for the range of G covered in these experiments (a factor of about 20), the power law (5) describes well this dependence at the top of the heat-injection zone. Velocity measurements show that at the higher values of G the jet accelerates in the upper heat-injection and lower post-heating zones; and that, while the turbulence intensity increases, the normalized value decreases by about 35%. However, no such drastic dependence on the heating is found in the normalized profile of either mean dye concentration or mean velocity.

4.5. *Analysis of the experimental data*

One of the main objectives of the present experiments is to understand the nature of the entrainment when there is local heating in the flow. How does the value of the entrainment coefficient (say α_E) in the locally heated jet compare with that for a neutral jet or a plume? Accurate measurement of the velocity across the jet at several axial positions is required to obtain entrainment from experimental data. Flow towards the edges of the jet is highly intermittent and long averaging times are required to get the mean velocities accurately; this is difficult and extremely time-consuming in experiments of relatively short duration of the kind reported here. We therefore estimate the entrainment from measured quantities indirectly: indeed the observations described in §4 have immediate and important consequences for the entrainment into the heated jet.

To see this, let us consider the case $G = 4.7$ in figure 6, for which the (dye concentration) jet width b can be treated as virtually constant over the region $150 < z/d < 200$. Assuming for the moment that β, the ratio of the scalar concentration to the velocity jet width, is constant (the present experiments indicate a value of about 1.3 for the unheated jet), and given that the mean velocity profiles always obey similarity very closely on local scales, the quantity $M = b^2 U_c$ gives a measure of the local mass flux (since density variations are negligible). Furthermore, if we assume that Taylor's entrainment hypothesis is valid and so the value of the entrainment coefficient α_E is not affected by heating, the continuity equation

$$\frac{\mathrm{d}}{\mathrm{d}z}(b^2 U_c) = 2\alpha_E b U_c \tag{6}$$

predicts that the centreline velocity in the region where b is constant must be given by

$$U_c(z) = U_c(z_1)\exp[2\alpha_E(z - z_1)/b(z_1)], \tag{7}$$

where z_1 is the axial distance from the station where the jet width $b(z_1)$ assumes a constant value.

Values of M, calculated from the experimental data for b and U_c, and those predicted by equation (7), are shown in figure 10. The variation of M in the preheating zone is predicted well by equation (7) for $\alpha_E = 0.09$. While the experimental estimate shows little or no increase in M in the region in question, that predicted by (7) would show a considerable increase, even when α_E is taken as low as 0.05 (from the value which may be thought consistent with observation in the lower heat-injection zone). These differences are well beyond the range of uncertainty of the data. Estimates of mass flux from measured velocity profiles show the same qualitative trend (Elavarasan *et al.* 1995), but are subject to some uncertainty because the data are available only at three points after commencement of heat injection, and velocities at the edges of the jet, which make a not-insignificant contribution to the mass flux, are hard to measure because of their low values. Both sets of data however lead to the unavoidable conclusion that the assumption of constant α_E is not at all realistic in the heat-injection zone, and indeed that it suffers a drastic reduction at high values of the heating parameter.

Now it has been suggested that for flows where equilibrium (self-similarity) has not been established, entrainment should be related not to the mean velocity but to the Reynolds stress (Morton 1968) or local level of turbulence (Telford 1975). As already shown, the latter does not decrease in absolute magnitude so the corresponding hypothesis would not be tenable either. It therefore seems clear that the explanation has to be found in the major structural changes that the flow experiences with heat injection.

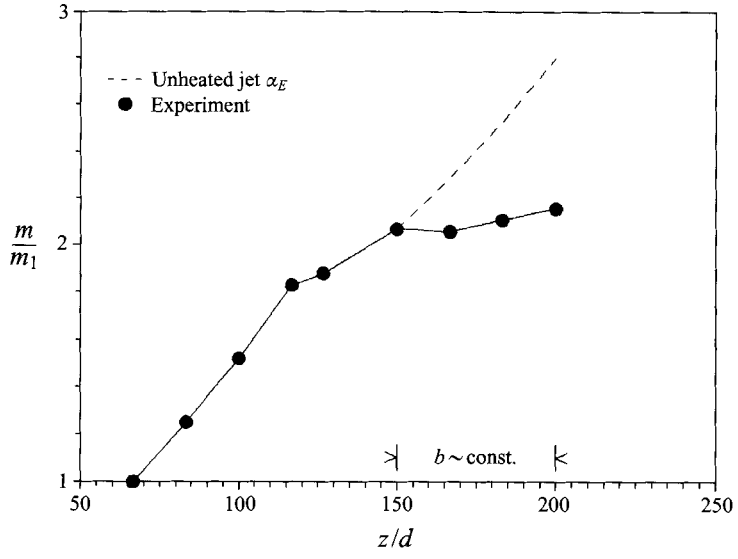

FIGURE 10. Predicted and experimentally measured specific mass flux in the region of the jet where the jet scalar width is nearly constant.

5. An integral model for the locally heated jet

We now devise an integral model that attempts to describe the development of the jet with local heating. The model is based on the (integral) conservation equations for mass, momentum, energy and scalar (i.e. acid) concentration. As suggested from the discussion above, treating the various coefficients that appear in the model as constants is not reasonable. However, when we allow the coefficients to vary, the number of unknowns can become numerous. Our main objective here is to outline the considerations that would have to be incorporated in models that aim to reproduce at least the gross features of the flow. To do this we use results from experiments in which, under nearly identical conditions, both LDV and scalar concentration data were taken, so both the axial velocity U_c and jet width b are available as functions of z; for example, flow conditions corresponding to $G = 0.5$ and 4.7 in figure 6 are respectively comparable to the cases $G = 0.5$ and 4.2 in figure 9(a). Our approach here is to solve the model equations (see below) using a smooth curve fitted to the measured concentration width (figure 6) as an input to the model; the conditions under which the predicted and measured velocities agree can give us a clue to the situation prevailing in the heated jet.

The conservation equations for the present axisymmetric jet, under the Boussinesq approximation, are

$$\frac{\mathrm{d}}{\mathrm{d}z}\int_0^\infty u r \mathrm{d}r = \frac{E}{2\pi} \quad \text{(continuity)}, \tag{8}$$

$$\frac{\mathrm{d}}{\mathrm{d}z}\int_0^\infty u^2 r \mathrm{d}r = g\alpha \int_0^\infty \theta r \mathrm{d}r \quad \text{(axial momentum)}, \tag{9}$$

$$\frac{\mathrm{d}}{\mathrm{d}z}\int_0^\infty u c r \mathrm{d}r = 0 \quad \text{(scalar concentration)}, \tag{10}$$

$$\frac{\mathrm{d}}{\mathrm{d}z}\int_0^\infty ur\theta \mathrm{d}r = \frac{Q}{\pi I_o}\frac{1}{\rho C_p}\int_0^\infty cr\mathrm{d}r \quad (z_b \leqslant z \leqslant z_t)$$
$$= 0 \qquad \text{otherwise (heat energy)}, \tag{11}$$

where

$$I_o = \int_{z_b}^{z_t} b^2 c_c \mathrm{d}z, \tag{12}$$

$$-E = \lim_{r\to\infty} 2\pi vr \quad \text{(entrainment/length)},$$

u is the axial component of the velocity, v the radial component, c the acid concentration, Q the net heating rate, θ the temperature excess over the ambient value and α the coefficient of thermal expansion. In (11) it is assumed that the local heating rate is proportional to the local acid concentration, and that its integral over the entire heat-injection zone yields the total heat-injection rate Q. Assuming self-similar profiles in the horizontal, the above equations can be reduced to the following set of ordinary differential equations:

$$\frac{\mathrm{d}b}{\mathrm{d}z} = \frac{g\alpha f_0 \theta_c b}{2f_1 U_c^2} - \frac{b}{U_c}\frac{\mathrm{d}U_c}{\mathrm{d}z} - \frac{b}{2f_1}\frac{\mathrm{d}f_1}{\mathrm{d}z}, \tag{13}$$

$$\frac{\mathrm{d}U_c}{\mathrm{d}z} = \frac{g\alpha f_0 \theta_c}{2f_1 U_c} - \frac{U_c}{b}\frac{\mathrm{d}b}{\mathrm{d}z} - \frac{U_c}{2f_1}\frac{\mathrm{d}f_1}{\mathrm{d}z}, \tag{14}$$

$$\frac{\mathrm{d}c_c}{\mathrm{d}z} = \frac{ec_c}{b^2 U_c} - \frac{c_c}{f_2}\frac{\mathrm{d}f_2}{\mathrm{d}z}, \tag{15}$$

$$\frac{\mathrm{d}\theta_c}{\mathrm{d}z} = \frac{f_4}{f_3}\frac{c_c}{U_c} - \frac{e\theta_c}{b^2 U_c} - \frac{\theta_c \mathrm{d}f_3}{f_3 \mathrm{d}z}, \tag{16}$$

where U_c and b are respectively local centreline velocity and half-width, and

$$e = \frac{\mathrm{d}}{\mathrm{d}z}(b^2 U_c).$$

The subscript c refers to the values on the jet centreline; the f_i, $i = 0, 1, 2, 3$, are coefficients defined by the integrals

$$f_0 = \int_0^\infty (\theta/\theta_c)\eta \mathrm{d}\eta, \quad f_1 = \int_0^\infty \left[\left(\frac{U}{U_c}\right)^2 + \frac{\overline{u'^2}}{U_c^2}\right]\eta \mathrm{d}\eta,$$

$$f_2 = \int_0^\infty \left[\frac{U}{U_c}\frac{c}{c_c} + \frac{\overline{u'c'}}{U_c c_c}\right]\eta \mathrm{d}\eta, \quad f_3 = \int_0^\infty \left[\frac{U}{U_c}\frac{\theta}{\theta_c} + \frac{\overline{u'\theta'}}{U_c \theta_c}\right]\eta \mathrm{d}\eta,$$

$$f_4 = \frac{Q}{\pi I_o \rho c_p}\int_0^\infty \frac{c}{c_c}\eta \mathrm{d}\eta, \quad \eta \equiv r/b.$$

Assuming Gaussian profiles for axial velocity and acid concentration, and either a Gaussian or a top-hat profile for the temperature distribution, the above equations are solved numerically. Results show that when the coefficients f_i are held constant, the velocities U_c are over-predicted (see figure 13). Allowing for a decrease in turbulent transport in the heat-injection zone does not improve the results noticeably. As we have seen in §4.3, data from image processing and LDV indicate that, when normalized by the local scales, the profiles of axial velocity and concentration are both self-similar. Therefore we are forced to consider the variation of β, the ratio of scalar to velocity width, as a possible factor in explaining the present data.

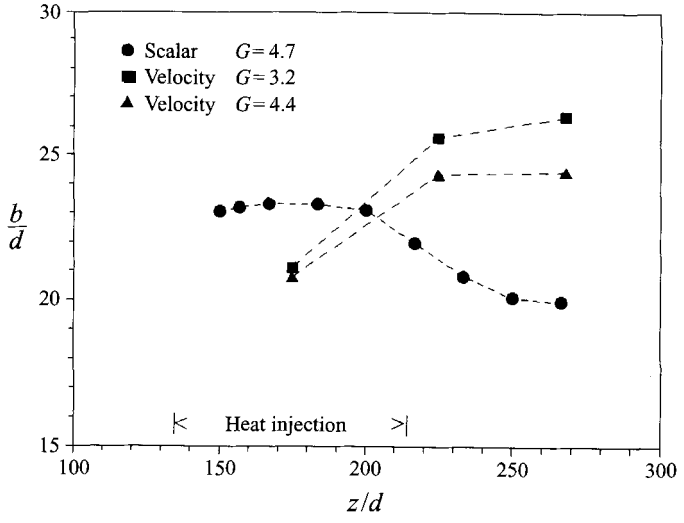

FIGURE 11. Axial variation of velocity and scalar jet widths for a heated jet.

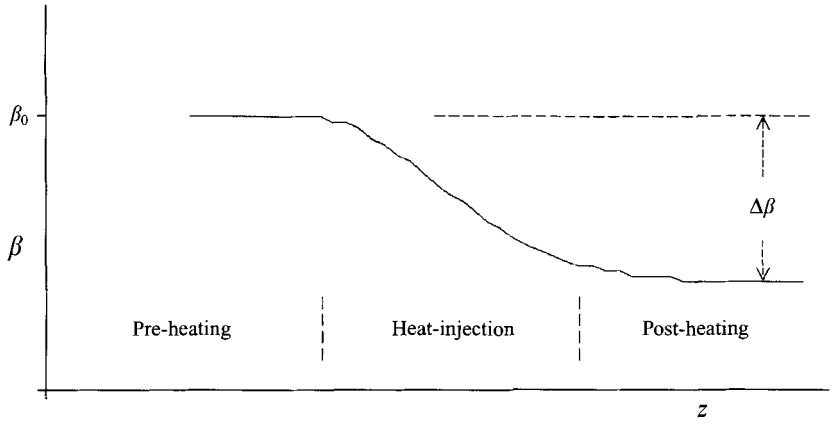

FIGURE 12. A schematic of the variation of β in the heated jet. The form adopted in the calculations is (i) $\beta = \beta_0$, $z \leqslant z_b$, (ii) $\beta = \beta_0 - \Delta\beta\{1 - \exp[-\lambda(z - z_b)^2/L^2]\}$, $z > z_b$. L basically represents the length scale for β-variation in the heat-injection zone.

Now figure 11 compares velocity and scalar jet widths for a heated jet for which both data are available. It is seen that, following volumetric heating, the growth rate of each width slows down; however, the scalar width is affected earlier than the velocity width, indicating a decrease in β. The few data points available are not sufficient to suggest the precise nature of the variation of β. On physical grounds it is reasonable to expect that β depends on z' (the axial distance from z_b) and on the heating parameter G; and that it approaches some constant value as either z' or G becomes large. There are several functions that have these properties, and one such form is shown in figure 12. The coefficient λ there is assumed to depend on G as

$$\lambda = G^m. \tag{17}$$

Figure 13 shows the jet centreline velocity predicted by the model. It is seen that when β is allowed to decrease in the heat-injection zone, the predicted velocities are

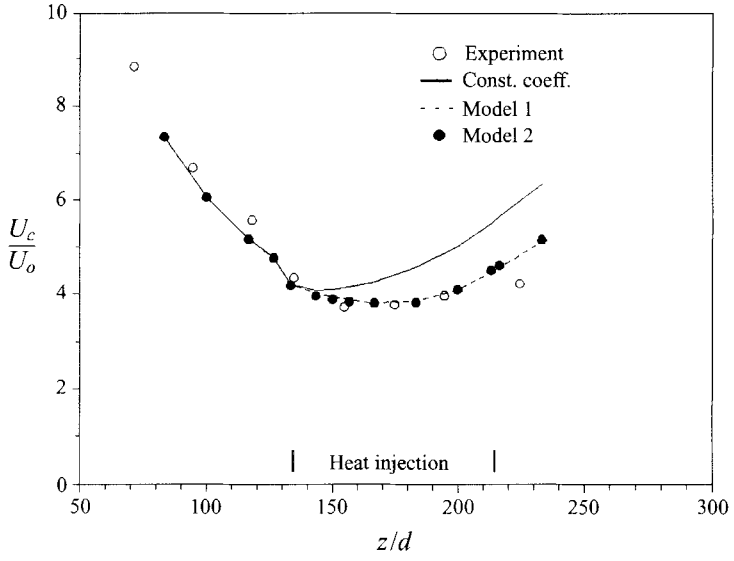

FIGURE 13. Comparison of measured and predicted variation of mean jet centreline velocity at a heating rate of 750 W and jet inlet velocity of 1 $\mathrm{m\,s^{-1}}$ ($G \simeq 4.2$). $\beta_0 = 1.25$, $\Delta\beta = 0.2$ and $L = 0.08$ m. Model 1 is that given in figure 12; model 2 assumes a linear variation of β with z decreasing from 1.25 to 1.05 over an axial distance of 0.08 m from z_b and remaining constant thereafter.

in better agreement with the experimental measurements. It turns out that the model predictions are not very sensitive to the precise form of the variation of β, because a linear decrease in the heat-injection zone yields results not very different from those in figure 12.

So the tentative conclusion from this exercise is that a major reason for the failure of early integral models for flows with volumetric heating is that the variation of β has not been taken into account. Further work is needed before a convincing model that allows for variable β can be formulated.

6. Mechanism responsible for disrupting the large-eddy structure

The significant changes in entrainment following heat injection into the jet call for an explanation of the possible mechanisms involved. Of course any model for turbulent shear flow, i.e. the stresses within it, yields a prediction for the evolution of the flow, and hence by implication for the entrainment. In general, such predictions are in the direction suggested by the entrainment hypothesis mentioned in §1. J. C. R. Hunt (1995, personal communication) has recently introduced a new hypothesis according to which the rate of growth of the cross-sectional area of the flow is largely controlled by the large-scale turbulence fluctuations in the flow, and showed how under certain conditions entrainment could decrease downstream. For example, entrainment into a plume could decrease or even become negative in the presence of external turbulence.

However, the experimental data presented in §4 argue against a direct connection between entrainment and flow kinetic energy – in either the mean or the fluctuating motion – as the entrainment decreases while the energies either do not decrease or may actually even increase.

We are therefore compelled to explore here an alternative explanation, which

suggests that entrainment, especially in free shear flows, is largely the result of engulfment of outer irrotational flow due to the induced velocity field of large-scale vortical structures present in the shear flow; the fluid so ingested is enfolded within the structure, and finally, through the action of small eddies and diffusion, gets mixed at the molecular level with the rotational fluid in the flow (see e.g. Roshko 1993; Hussain 1986).

Now the organization of the vortical structures characterizing a round turbulent jet is not as evident from flow visualization pictures as in mixing layers, but nevertheless there is evidence to suggest that a spiral or helical structure plays a key role. Tso & Hussain (1989) find the dominant structure to be a single helix, but a double helix and a ring-like structure were also found. Dahm & Dimotakis (1990) show laser-induced flourescence pictures suggesting a spiral structure at relatively low Reynolds numbers, and an ordered sequence of arrow-head-shaped regions within which the composition of dyed fluid shows little variation; a similar shape was already in evidence in the schlieren photographs presented in the early work of Crow & Champagne (1971). The experimental evidence indicates that the engulfment takes place around the broad base at the upstream end of the structure, and that there is strong mixing activity near the tip of the arrow. A related proposal has been made more recently by Yoda, Hesselink & Mungal (1992, 1994). (We would incidentally propose here that a structure that is consistent with the arrow-head-shaped region and the spiral vortex would be a closed loop with a fragment of a vortex ring at the base that twists up in a spiral to the head and twists back to the base again.)

Now we have already presented visual evidence in figures 3 and 4 that the injection of heat in the present experiment destroys the structure characteristic of the unheated jet. As the instantaneous concentration of a passive scalar tends to vary little across a structure (Dahm & Dimotakis 1990), this should be true of acid concentration as well in the present experiment. This means that whenever such structures are passing by, the electrical resistance decreases locally (since the central eddies carry more acid in them), and correspondingly the heating is also nearly uniform across. As the velocity distribution across the structure is however non-uniform, the instantaneous temperature would be larger towards the outer region of the jet. As a result, a larger body force would act in this region and the flow considerably distorted; and the disruption of the structure noted above becomes understandable. The immediate consequence is that the engulfing action of the vortical structure in the flow is no longer operational, and consequently the entrainment is disabled.

The following considerations make the above argument more specific.

The estimated maximum rise in the temperature at the highest value of G used in the experiments is about 4°C, the corresponding fractional decrease in the density is about 10^{-3}, and the estimated bulk Richardson number is about 0.2 (at a typical velocity $U_c = 5\ \mathrm{cm\,s^{-1}}$ and a length scale H of 6 cm), which may at first sight be taken to suggest that inertia forces nominally remain large compared to buoyancy forces. However the experiments indicate that the jet is affected much more than the low average value of the Richardson number suggests. In the experiments by Hermanson & Dimotakis (1989) the Richardson number is about 0.004, a value at which the effects of buoyancy are normally considered to be unimportant; however, there is considerable reduction in entrainment. Therefore, it appears that the volumetric heating does much more than merely bringing modest buoyancy forces into play in the mean momentum balance.

A plausible mechanism for the large influence is the following. Consider a small

parcel of buoyant fluid moving up and accelerating in the ambient. Neglecting viscous effects, the momentum equation governing the motion of the parcel is

$$\frac{\mathrm{d}w}{\mathrm{d}t} = \frac{g(\rho_a - \rho_p)}{\rho_p}, = g' \text{ say}, \tag{18}$$

where w is the vertical velocity and the subscripts a and p refer to ambient and parcel fluid respectively. Integrating (18) from an initial height z_1 with an initial vertical velocity w_1 to a height z, we get

$$w = [w_1^2 + g'(z - z_1)]^{1/2}. \tag{19}$$

Now consider a coherent structure in which the fluid is warmer than the ambient by 1°C. When the structure moves up by 1 cm, the increase in fluid velocity is 0.45 cm s^{-1} if it starts from rest and 0.02 cm s^{-1} if it had an initial velocity of 4 cm s^{-1}: these initial velocities roughly correspond to fluid velocities near the outer edge ($r = 2b$) and the axis of the jet respectively in the heat-injection zone in the present experiments. Therefore, between any two given stations, a given increase in temperature has a far more pronounced effect on the fluid velocity towards the edge of the jet than near the axis.

Now although the precise effect of the heating will probably depend on its distribution across the jet, it is clear from the above argument that, if only because of the velocity variation across the flow, such heating will affect the flow differently at different radii. This differential influence will disrupt the prevailing coherent structure, in particular its toroidal base that appears to be the seat of vigorous induced motion of external fluid, and consequently diminish the entrainment at the very initial stage of the process, namely engulfment. Because of this, the bulk Richardson number which is usually based on the jet centreline velocity plays down the role of buoyancy in such situations. It is remarkable that the effect of heating is so marked, even though the energy contained in the coherent motion in a turbulent jet is estimated to be only about 10% (to be compared with about 20% in mixing layers; see Fiedler 1987). This suggests that the disruption of the organization of the structure must be a key element of the entrainment reduction process.

We finally note that the diminution in entrainment noted above may equivalently be attributed to the acceleration that occurs on heating. In both boundary layers (Narasimha & Sreenivasan 1973) and wakes (Prabhu, Narasimha & Sreenivasan 1974), acceleration (in these cases imposed through the free stream) has a similar effect. The explanation through the disruption of coherent structures is certainly valid in the accelerated boundary layer as well, and there is no reason to expect it is different in the wake.

7. Relevance of the present experiments to clouds

We should like to discuss briefly the implications of the present experiment for entrainment in cumulus clouds.

As already pointed out in §1, the inability of the laterally entraining one-dimensional plume model to predict properties of cumulus clouds has long been recognized. In particular, if such a model is tuned to match the observed liquid-water content, the resulting air is too cold to ascend to the observed cloud heights; if tuned to match the observed cloud tops, the liquid-water content is over-predicted (e.g. Warner 1970). Further, for laterally entraining plumes and thermals, velocity and length scales are negatively correlated (Turner 1973); however there is no clear observational support for such a tendency in cumulus and cumulonimbus clouds (e.g. LeMone & Zipser

1980). Analysis of *in-situ* measured temperature and liquid-water content in non-precipitating cumulus clouds shows that some air within these clouds ascends all the way from cloud base to cloud top undiluted by ambient air (Paluch 1979). In fact, the composition of cloud air near the cloud top shows that it results from mixing of the air from cloud base and the ambient air near cloud top (cloud top entrainment); only in regions much below the cloud top is there evidence for lateral mixing (LaMontagne & Telford 1983). Therefore, the flow inside clouds is very different from that in classical jets and plumes where the ambient air is continuously drawn into the flow and mixed thoroughly.

On the other hand, it is now well known from many laboratory studies, including the present one, that coherent structures in turbulent shear flows are responsible for entrainment. Consequently any change in the large-eddy structure is bound to affect the lateral entrainment of ambient fluid into the flow. Such a change occurs in clouds due to the volumetric heat release and absorption associated with the phase change of water, and the resulting enhancement of the buoyancy of the cloud air in the direction of the flow. We attribute the failure of the standard plume model to the neglect of the effect of such heat release on coherent structures and entrainment.

Based on our experience with the volumetrically heated jet, we propose the following tentative scenario in cumulus clouds. Since the cloud base remains more or less at the same height as the cloud grows in the vertical, a starting plume (Turner 1973, p. 191) is perhaps the closest laboratory model that describes the gross (external) features of a cloud. Imagine air inside a starting plume getting saturated at a certain height (the cloud base). A schematic of the large-eddy structure of the flow at this stage is shown in figure 14*a* (Turner 1973, p. 166). As the air ascends further, condensation of water vapour releases latent heat, enhancing the buoyancy of the cloud air (at warm temperatures the heating due to phase change more than compensates for the cooling due to adiabatic expansion resulting in net buoyancy increase, e.g. Iribarne & Godson 1973, pp. 158–159). The lateral extent of the cloud varies from a few hundred metres to few kilometres (e.g. Ludlam 1980). The vertical velocity near the cloud base is typically less than 3 $\mathrm{m\,s^{-1}}$ (LeMone & Zipser 1980; Warner 1977), and the fluctuations over distances much smaller than the size of the cloud are comparable to the vertical velocity (Warner 1977). This allows sufficient time for the smaller eddies to mix some amount of ambient and cloud air within one large-eddy turnover time. The mixture of cloud and ambient air adjacent to it (that is usually dry, i.e. has low relative humidity) can be colder than the airs that are being mixed (Ludlam 1980, p. 54). Increased liquid-water content of cloud air and drier ambient air enhance evaporative cooling. Therefore, even before the large eddy can draw the ambient fluid deep into the flow, part of the mixed air may have negative buoyancy and generate downward motion. Hence, after some distance above the cloud base, the flow associated with a cloud may appear as shown in figure 14(*b*). Note that buoyancy enhancement due to latent heat release will by itself disrupt the large-eddy structure of the cloud; the evaporative cooling accelerates this disruption process further. It is conceivable that most of whatever ambient air is entrained by the cloud would not penetrate to its core – instead, it may come down in downdraughts near the cloud edges. Once the large eddy is broken, large-scale engulfment of ambient air will cease, and lateral mixing further downstream may be limited to the outer edges of the cloud; fluid in the central core will ascend practically undiluted by the ambient air.

The scenario presented above is fully consistent with the observed behaviour of clouds.

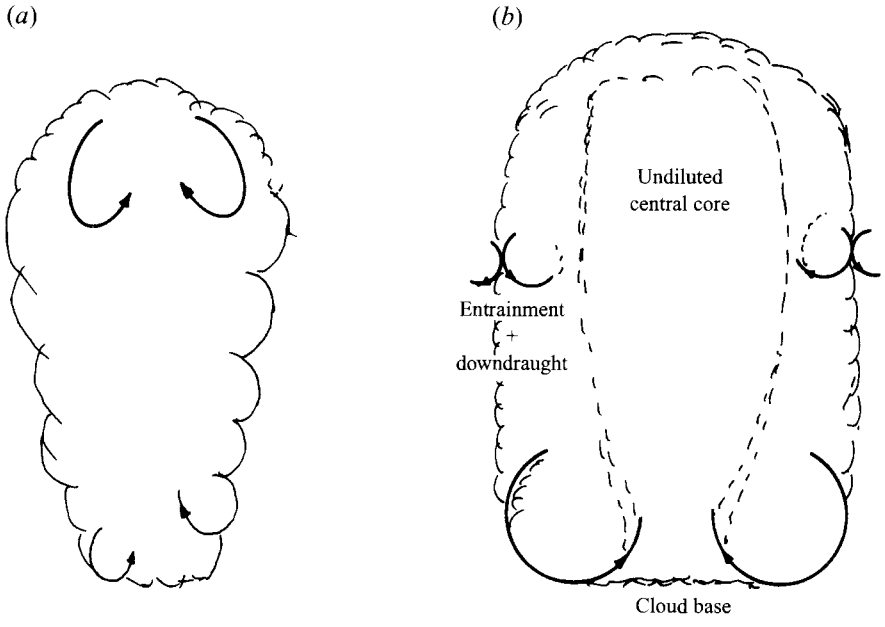

FIGURE 14. Schematic of a hypothetical large-eddy structure of a starting plume in the atmosphere. (*a*) Classical flow (Turner 1973, p. 166). (*b*) Flow with phase change of water. The horizontal extent of the large eddies decreases due to the buoyancy enhancement in the direction of the flow following the phase change of water.

8. Conclusion

The present study has demonstrated that volumetric heating disrupts the jet eddy structure in the heat-injection zone, the jet spread rate reduces drastically, and even visually its behaviour is very different from that of a buoyant jet. From measurements of the jet-width variation it is seen that the parameter G, which is a measure of the ratio of buoyancy to inertial forces in the present problem, plays a key role in determining jet behaviour. As G increases, the normalized turbulence intensity decreases by as much as 35% in the heat injection zone but gradually increases thereafter in the post-heating zone as the flow relaxes towards equilibrium again. Analysis of the experimental data suggests that Taylor's entrainment hypothesis, with a constant value of entrainment coefficient, is not valid in and just beyond the heat-injection zone. It is proposed here, based on the evidence of flow visualization, that the disruption of coherent structures due to heating is responsible for a drastic reduction in entrainment, and explains the failure of entraining plume models for clouds.

This work was largely supported through grants from the Department of Science and Technology, New Delhi and the Extra Mural Division, Council of Scientific and Industrial Research, New Delhi. The authors appreciate the grants provided and sincerely thank these agencies. A small grant from the Jawaharlal Nehru Centre at a critical time was most helpful. Authors also thank Dr. R. Elavarasan for assistance in conducting the experiments, especially the LDV measurements, Prof. A. Prabhu for sparing the Argon-ion laser and the LDV system for these experiments, and Mr L. Venkatakrishnan for help in taking flow visualization pictures.

Appendix. Error in the estimation of jet width due to variation in ϕ and I_e

A fluorescent dye absorbs light energy in some wavelength range and emits radiation at longer wavelengths, uniformly in all directions. The fluorescence intensity received at a suitably located detector is given by (e.g. Walker 1987)

$$I_f = K\phi\epsilon c(s)I_e(s)\mathrm{d}s \tag{A 1}$$

where K is the fraction of the available fluorescence light energy collected at the detector, ϕ is the quantum efficiency of the dye, ϵ is dye absorptivity or extinction coefficient, c is dye concentration, I_e is the exciting light intensity, and s is the distance measured in the direction of light propagation. Equation (A1) is the basis for quantitative measurements. A linear response between c and I_f is observed for values of c up to about 100 $\mu\mathrm{g\,ml^{-1}}$, but as the dye concentration increases, a process known as quenching takes place and (A1) will not be valid (Guilbault 1973, p. 19). Another aspect that needs attention in the present study, because of the temperature differences in the jet, is the observation that, other conditions remaining the same, I_f decreases with increasing temperature.

First let us consider the variation in the exciting light intensity in the incident laser beam (Gaussian in $\mathrm{TEM_{00}}$ mode) and that due to the divergence caused by the cylindrical lens. In the present experiments, the cylindrical lens has a diameter of 7 mm and is placed at a distance of 1300 mm from the jet axis. Using the laws of geometric optics, ray paths emerging from the cylindrical lens have been calculated. Assuming that the incident laser beam is symmetrically placed with respect to the lens, incident intensity for each ray has been obtained from the Gaussian distribution. Light intensity decreases as the rays diverge, and, for a given ray, the relative intensity at any point along its path is taken to be inversely proportional to the separation between its two neighbouring rays. For the distance covered in the present experiments (about 150 mm on either side of the laser sheet axis, i.e. covering an axial distance of 300 mm along the jet) the intensity variation in the light sheet relative to the value on the jet axis within a horizontal distance of 50 mm from it is found to be within 1%. Let

$$I_e(r,z) = aI_e(0,z) = aI_{ec}. \tag{A 2}$$

It may be noted from figure 5 that the observed jet width is generally less than 50 mm; therefore the lowest value of a in (A2) is expected to be about 0.99.

Next let us consider the change in the quantum efficiency ϕ due to temperature variation across any horizontal section. We may express ϕ as

$$\phi(T) = \phi(T_c)[1 - \alpha_\phi(T - T_c)] \tag{A 3}$$

where T_c is the temperature at the jet centreline and α_ϕ is the fractional change in ϕ due to a unit change in temperature. For the flow conditions used in the present experiments, $(T - T_c)$ is at most 4°C (in most cases less than 2°C). Assuming $\alpha = 1\%$ (see Guilbault 1971, p. 24), equation (A3) suggests that the change in ϕ across the jet is less than 4%.

Now for a given fluorescent dye and recording arrangement, the fluorescent intensity measured at a grid point can be expressed using (A1) as

$$I_f = K_1\phi(T)c(r,z)I_e(r,z); \tag{A 4}$$

its value on the jet axis ($r = 0$, denoted by subscript c) is

$$I_{fc} = K_1\phi(T_c)c_c(z)I_{ec}. \tag{A 5}$$

Using relations (A2) to (A5), the measured intensity corresponding to any point (r, z) in the plane can be expressed as

$$I_f = K_1\phi(T_c)[1 - \alpha_\phi(T - T_c)]c_c(z)\mathrm{e}^{-(r/b)^2}aI_{ec} \tag{A 6}$$

$$= a[1 - \alpha_\phi(T - T_c)]I_{fc}\mathrm{e}^{-(r/b)^2}, \tag{A 7}$$

where a Gaussian distribution having a width b is assumed for the dye concentration variation across the jet. The jet width b_1 measured in the present work is based on the relation

$$I_f = I_{fc}\mathrm{e}^{-(r/b_1)^2}. \tag{A 8}$$

Comparing (A7) and (A8) at $r = b_1$ and after some rearrangement, we get

$$b_1/b = [1 - \ln\ y]^{1/2} \tag{A 9}$$

where $y = a[1-\alpha_\phi(T-T_c)]$. In the present experiments, y is found to be not less than 0.95. Assuming the worst case, i.e. $y = 0.95$, we get $b_1/b = 0.974$ from (A9). Therefore the maximum error in the measured scalar concentration width due to variations in ϕ and I_e is expected to be less than 2.5%.

REFERENCES

Bhat, G. S., Narasimha, R. & Arakeri, V. H. 1989 A new method of producing local enhancement of buoyancy in liquid flows. *Exps. Fluids* **7**, 99–102.

Broadwell, J. E. & Breidenthal, R. E. 1982 A simple model of mixing and chemical reaction in a turbulent shear flow. *J. Fluid Mech.* **125**, 397–410.

Crow, S. C. & Champagne, F. H. 1971 Orderly structure in jet turbulence. *J. Fluid Mech.* **48**, 547–591.

Dahm, W. J. A. & Dimotakis, P. E. 1990 Mixing at large Schmidt number in the self-similar far field of turbulent jets. *J. Fluid Mech.* **217**, 299–330.

Dimotakis, P. E., Miake-Lye, R. C. & Papantoniou, D. A. 1983 Structure and dynamics of round turbulent jets. *Phys. Fluids* **26**, 3185–3192.

Elavarasan, R, Bhat, G. S., Narasimha, R. & Prabhu, A. 1995 An experimental study of a jet with local buoyancy enhancement. *Fluid Dyn. Res.* **16**, 189–202.

Emanuel, K. A. 1994 *Atmospheric Convection.* Oxford University Press.

Fiedler, H. E. 1987 Coherent structures. In *Advances in Turbulence, Proc. 1st Euro. Turb. Conf., Lyon 1986*, pp. 320–336. Springer.

Fox, D. G. 1970 Forced plume in a stratified fluid. *J. Geophys. Res.* **75**, 6818–6835.

Guilbault, G. C. 1973 *Practical Fluorescence.* Marcel Dekker.

Gutmark, E. & Ho, C. M. 1983 Preferred modes and spreading rates of jets. *Phys. Fluids* **26**, 2932–2938.

Hermanson, J. C. & Dimotakis, P. E. 1989 Effects of heat release in a turbulent shear layer. *J. Fluid Mech.* **199**, 333–375.

Hirst, E. 1972 Zone of flow establishment for round buoyant jets. *Water Resources Res.* **8**, 1234–1246.

Hunt, J. C. R. 1993 Atmospheric jets and plumes. In *Recent Research Advances in the Fluid Mechanics of Turbulent Jets and Plumes* Proc. NATO Advanced Study Institute, Viano di Castelo, pp. 309–334. Kluwer.

Hussain, F. 1986 Coherent structures and turbulence. *J. Fluid Mech.* **173**, 303–356.

Hussein, J. H., Capp. S. P. & George, H. K. 1994 Velocity measurements in a high-Reynolds-number, momentum-conserving, axisymmetric turbulent jet. *J. Fluid Mech.* **258**, 31–75.

Iribarne, J. V. & Godson, W. L. 1973 *Atmospheric Thermodynamics.* D. Reidel.

LaMontagne, R. G. & Telford, J. W. 1983 Cloud top mixing in small cumuli. *J. Atmos. Sci.* **40**, 2148–2156.

LeMone, M. A. & Zipser, E. 1980 Cumulonimbus vertical velocity events in GATE. Part I: diameter, intensity, and mass flux. *J. Atmos. Sci.* **37**, 2444–2457.

LIEPMANN, D. & GHARIB, M. 1992 The role of streamwise vorticity in the near-field entrainment of round jets. *J. Fluid Mech.* **245**, 643–668.

LIST, E. J. & IMBERGER, J. 1973 Turbulent entrainment in buoyant jets and plumes. *J. Hydraul. Div. ASCE* **99**, 1461–1474.

LUDLAM, F. H. 1980 *Clouds and Storms.* Pennsylvania University Press.

MORTON, B. R. 1968 Turbulent structure in cumulus models. *Intl Conf. on Cloud Physics, Toronto, Aug. 1968.*

MORTON, B. R., TAYLOR, G. I. & TURNER, J. S. 1956 Turbulent gravitational convection from maintained and instantaneous sources. *Proc. R. Soc. Lond.* A **234**, 1–23.

NARASIMHA, R. & PRABHU, A. 1972 Equilibrium and relaxation in turbulent wakes. *J. Fluid Mech.* **54**, 1–17.

NARASIMHA, R. & SREENIVASAN, K. R. 1973 Relaminarization in highly accelerated turbulent boundary layers. *J. Fluid Mech.* **61**, 417–447.

PALUCH, I. R. 1979 The entrainment mechanism in Colorado cumuli. *J. Atmos. Sci.* **36**, 2467–2478.

PAPANICOLAOU, P. N. & LIST, E. J. 1988 Investigations of round vertical turbulent buoyant jets. *J. Fluid Mech.* **195**, 341–391.

PAPANTONIOU, D. & LIST, E. J. 1989 Large-scale structure in the far field of buoyant jets. *J. Fluid Mech.* **209**, 151–190.

PRABHU, A., NARASIMHA, R. & SREENIVASAN, K. R. 1974 Distorted wakes. *Adv. Geophys.* **18B**, 317–328.

RICOU, F. P. & SPALDING, D. B. 1961 Measurements of entrainment by axisymmetrical turbulent jets. *J. Fluid Mech.* **11**, 21–32.

RIEHL, H. 1979 *Climate and Weather in the Tropics.* Academic Press.

ROSHKO, A. 1976 Structure of turbulent shear flows: a new look. *AIAA J.* **14**, 1349–1357.

ROSHKO, A. 1993 Instability and turbulence in shear flows. In *Theoretical and Applied Mechanics 1992.* Elsevier.

SIMPSON, J. 1983 Cumulus clouds: early aircraft observations and entrainment hypotheses. In *Mesoscale Meteorology* (ed. D. K. Lilly & T. Gal-Chen), pp. 355–445. D.Reidel.

SQUIRES, P. & TURNER, J. S. 1962 An entraining jet model for cumulonimbus updrafts. *Tellus* **14**, 422–434.

TELFORD, J. W. 1975 Turbulence, entrainment, and mixing in cloud dynamics. *PAGEOPH* **113**, 1067–1084.

TOWNSEND, A. A. 1976 *The Structure of Turbulent Shear Flow*, 2nd edn. Cambridge University Press.

TSO, J. & HUSSAIN, F. 1989 Organised motions in a fully developed turbulent axisymmetric jet. *J. Fluid Mech.* **203**, 425–448.

TURNER, J. S. 1973 *Buoyancy Effects in Fluids.* Cambridge University Press.

TURNER, J. S. 1986 Turbulent entrainment: the development of entrainment assumption and its application to geophysical flows. *J. Fluid Mech.* **173**, 431–471.

VISWANATH, P. R., NARASIMHA, R. & PRABHU, A. 1978 Visualization of relaminarizing flows. *J. Indian Inst. Sci.* **60**, 159–165.

WALKER, D. A. 1987 A fluorescence technique for measurement of concentration in mixing liquids. *J. Phys.* E: *Sci. Instrum.* **20**, 217–224.

WARNER, J. 1970 On steady-state one-dimensional models of cumulus convection. *J. Atmos. Sci.* **27**, 1035–1040.

WARNER, J. 1977 Time variation of updraft and water content in small cumulus clouds. *J. Atmos. Sci.* **34**, 1306–1312.

WYGNANSKI, L. & FIEDLER, H. 1969 Some measurements in the self-preserving jet. *J. Fluid Mech.* **38**, 577–612.

YODA, M., HESSELINK, L. & MUNGAL, M. G. 1992 The evolution and nature of large-scale structures in the turbulent jet. *Phys. Fluids* A **4**, 803–811.

YODA, M., HESSELINK, L. & MUNGAL, M. G. 1994 Instantaneous three-dimensional concentration measurements in the self-similar region of a round high-Schmidt-number jet. *J. Fluid Mech.* **279**, 313–350.